Journal of Scientific Computing (2019) 81:898–922
https://doi.org/10.1007/s10915-019-01042-w

Modified Stencil Approximations for Fifth-Order Weighted Essentially Non-oscillatory Schemes

Yahui Wang[1,2] · Yulong Du[3] · Kunlei Zhao[1,2] · Li Yuan[1,2]

Received: 19 January 2019 / Revised: 11 August 2019 / Accepted: 22 August 2019 /
Published online: 27 August 2019

Abstract
In this paper, a modified fifth-order weighted essentially non-oscillatory (WENO) finite difference scheme is presented. The quadratic polynomial approximation of numerical flux on each candidate stencil of the traditional WENO-JS scheme is modified by adding a form of cubic terms such that the resulting stencil approximation achieves fourth-order accuracy. And the corresponding smoothness indicators are calculated. The modified candidate fluxes and local smoothness indicators, when used in the WENO-JS scheme, can make the resulting new scheme (called WENO-MS) achieve fifth-order convergence in smooth regions including first-order critical points. A series of one- and two-dimensional numerical examples are presented to demonstrate the performance of the new scheme. The numerical results show that the proposed WENO-MS scheme provides a comparable or higher resolution of fine structures compared with the WENO-M, WENO-Z and P-WENO schemes, while it increases only 7% of CPU time compared with the traditional WENO-JS scheme.

Keywords WENO scheme · Stencil approximation order · Smoothness indicator · Hyperbolic conservation law · Euler equation

Mathematics Subject Classification 65M12 · 76L05 · 41A10

✉ Li Yuan
lyuan@lsec.cc.ac.cn

Yahui Wang
wangyh14@lsec.cc.ac.cn

Yulong Du
kunyu0918@163.com

Kunlei Zhao
klzhao@lsec.cc.ac.cn

1 ICMSEC and LSEC, Academy of Mathematics and Systems Science, Chinese Academy of Sciences, Beijing 100190, People's Republic of China

2 School of Mathematical Sciences, University of Chinese Academy of Sciences, Beijing 100190, People's Republic of China

3 School of Mathematics and Systems Science, Beihang University, Beijing 100191, People's Republic of China

1 Introduction

Essentially non-oscillatory (ENO) and weighted essentially non-oscillatory (WENO) schemes have been widely used for the numerical solution of hyperbolic conservation laws due to their high order accuracy in smooth region and essentially non-oscillatory behavior near discontinuity. An r-th order ENO scheme [1,2] is designed to choose the smoothest one from a set of r candidate stencils based on the local smoothness indicator of solution over a stencil. Liu et al. [3] first introduced the finite volume WENO scheme. The scheme uses a nonlinear convex combination of local r-th order approximations on all candidate stencils to achieve an $(r+1)$-th order accuracy in smooth regions while keeping the essentially non-oscillatory property of the ENO scheme near discontinuities. Jiang and Shu [4] introduced finite difference WENO schemes and gave a new smoothness indicator, which is the sum of the scaled L^2 norms of all derivatives of the polynomial approximation over a candidate stencil. The resultant fifth-order finite difference WENO scheme (hereafter denoted as WENO-JS) has become a quite successful methodology for solving multidimensional problems containing both strong discontinuities and complicated smooth solution structures in computational fluid dynamics. However, Henrick et al. [5] noticed that the actual convergence rate of the fifth-order WENO-JS scheme is 3 at critical points where the first derivative vanishes but the third derivative does not. Further, they derived the necessary and sufficient conditions on the weights for fifth-order convergence and developed the fifth-order WENO-M scheme by devising a mapping function for the weights of the WENO-JS scheme to satisfy the sufficient conditions. Borges et al. [6] proposed another fifth-order WENO scheme (WENO-Z) by utilizing a higher order global smoothness measurement to calculate the weights. The recommended WENO-Z scheme with the power parameter $p = 1$ has fourth-order accuracy at critical points of smooth solution, which is between 3 for the WENO-JS and 5 for the WENO-M schemes. Both WENO-M and WENO-Z schemes can obtain sharper results than the WENO-JS scheme when solving problems with shocks, mainly due to lager weights they assign to discontinuous stencils [6]. The WENO-Z scheme assigns even larger weights, obtaining even shaper solutions. And its CPU time cost is nearly the same as the WENO-JS scheme while the WENO-M scheme increases about 25% CPU time compared with the WENO-JS scheme. Later on, Ha et al. [7] developed the WENO-NS scheme by using a smoothness indicator based on the L^1 norm, and further improved their scheme by proposing adjustable nonlinear weights [8]. They shown that the resultant WENO-P scheme [8] has fifth-order accuracy even at critical points. However, the numerical results rely on two user-tunable parameters.

On the other hand, a few researchers [9–11] defined the parameter ε for preventing division by zero in the calculation of the WENO weights as a function of the mesh size Δx in order to obtain the optimal order at critical points. However, it is easy to see that if the reference length takes a small value, Δx will be a large value, and hence this kind of schemes lose the scale invariance property and are prone to generate numerical oscillations. Very recently, Zeng et al. [12] proposed the perturbational WENO (P-WENO) scheme by weighting the perturbed candidate fluxes with the weights of the WENO-Z scheme. They shown that the P-WENO scheme meets the necessary and sufficient conditions for fifth-order convergence even at critical points. In order to make the scheme have the ENO property, they used a tunable function to reduce the role of the additional flux correction terms. However, they used the same smoothness indicators as those of the WENO-JS scheme, which seem to be inconsistent with the 3rd-degree polynomial approximations over the candidate stencils implied by the numerical perturbation method they used.

In this article, based on the work of Zeng et al. [12], we propose a modified fifth-order WENO scheme. Unlike Ref. [12] which only gave the perturbed candidate flux at the grid interface $i+1/2$, we further construct the perturbed cubic polynomial approximation of the numerical flux on each candidate stencil. Then we compute the corresponding smoothness indicators according to the formula of the JS indicator. The high-order correction terms in the candidate numerical fluxes and smoothness indicators are limited by a tunable function in order to recover the ENO property as Ref. [12] did. And we only use the traditional WENO-JS weights instead of the delicate WENO-Z weights as in [12]. We call the resultant scheme WENO-MS scheme where "MS" stands for "modified stencil". We provide a theoretical analysis to show the fifth-order accuracy of the new scheme in smooth region including critical point. Some numerical experiments are presented to demonstrate that the WENO-MS scheme can obtain more salient results than the WENO-JS, WENO-M, WENO-Z and P-WENO schemes, while its CPU cost is only 7% more than the WENO-JS scheme.

The rest of this paper is organized as follows. Section 2 provides a brief review of the conservative fifth-order finite difference WENO scheme for one-dimensional scalar conservation laws including the necessary and sufficient conditions on the weights to achieve fifth-order convergence. In Sect. 3, the modified stencil approximation polynomials of the numerical flux are constructed, and the corresponding smoothness indicators are given. Then the WENO-MS scheme is presented and its order of convergence is analyzed. In Sect. 4 some numerical results are presented to show the performance of the present scheme. Finally, concluding remarks are given in Sect. 5.

2 Review of Finite Difference WENO Schemes

We consider the numerical solution of the one-dimensional scalar hyperbolic conservation law

$$u_t + f(u)_x = 0, \tag{1}$$

where $u(x,t)$ is the conservative variable, $f(u(x,t))$ is the flux function. Throughout this paper, we assume that a given domain $[a,b]$ is uniformly gridded with the set of cells $I_j := [x_{j-1/2}, x_{j+1/2}],\ j = 1,\ldots,N$. The center (node) of I_j is denoted by $x_j = (x_{j-1/2} + x_{j+1/2})$, and a function value at the node x_j is denoted by a subscript j, e.g., $f_j = f(x_j)$. The notion $\Delta x = (b-a)/N$ indicates the grid size.

Equation (1) can be approximated by the semi-discretization form

$$\frac{\mathrm{d}u_j}{\mathrm{d}t} = -\left.\frac{\partial f}{\partial x}\right|_{x=x_j}, \tag{2}$$

where $u_j(t)$ is the numerical approximation to the point value $u(x_j,t)$ at the node x_j. A conservative finite difference can be obtained by defining a numerical flux function $h(x)$ implicitly through the following equation [13]

$$f(x) = \frac{1}{\Delta x}\int_{x-\frac{\Delta x}{2}}^{x+\frac{\Delta x}{2}} h(\xi)\mathrm{d}\xi. \tag{3}$$

Differentiating (3) with respect to x shows that the derivative of f at x_j is equal to the conservative finite difference of the function $h(x)$ between cell interfaces exactly,

$$\left.\frac{\partial f}{\partial x}\right|_{x=x_j} = \frac{1}{\Delta x}\left[h\left(x_j + \frac{\Delta x}{2}\right) - h\left(x_j - \frac{\Delta x}{2}\right)\right]. \tag{4}$$

If $h_{j\pm1/2}$ in (4) is approximated by some numerical fluxes $\hat{f}_{j\pm1/2}$ to a high order, e.g., $h_{j\pm1/2} = \hat{f}_{j\pm1/2} + O(\Delta x^5)$, and the $O(\Delta x^5)$ term is smooth, then the approximation to the spatial derivative $(\partial f/\partial x)_{x=x_j}$ in (4) will have $O(\Delta x^5)$ accuracy [14]. For achieving numerical stability and avoiding entropy violating solutions, upwinding and flux splitting approaches are used in constructing the numerical flux. The original flux $f(u)$ is split into positive and negative fluxes, f^+ and f^-, so that

$$f(u) = f^+(u) + f^-(u), \tag{5}$$

where $\frac{\mathrm{d}f^+(u)}{\mathrm{d}u} \geq 0$ and $\frac{\mathrm{d}f^-(u)}{\mathrm{d}u} \leq 0$. One of the simplest flux splittings is the Lax–Friedrichs splitting which is given by

$$f^{\pm}(u) = \frac{1}{2}\left(f(u) \pm \alpha u\right), \tag{6}$$

where $\alpha = \max_u |f^{'}(u)|$ over the pertinent range of u. We then apply the WENO procedure to $f^{\pm}(u_j)$ to obtain the split numerical fluxes $\hat{f}^{\pm}_{j+1/2}$, and sum them up to obtain the numerical flux at the cell interface,

$$\hat{f}_{j+1/2} = \hat{f}^{+}_{j+1/2} + \hat{f}^{-}_{j+1/2}. \tag{7}$$

Hereafter, we will only describe how $\hat{f}^{+}_{j+1/2}$ is approximated because the formulas for $\hat{f}^{-}_{j+1/2}$ are symmetric to the positive counterparts with respect to $x_{j+1/2}$. Also, for simplicity, we will drop the "+" sign in the superscript.

2.1 Fifth-Order WENO Scheme

For constructing numerical flux $\hat{f}_{j+1/2}$ from known grid point values of f_j, the classic fifth-order WENO scheme uses a 5-point global stencil which is subdivided into three 3-point sub-stencils as shown in Fig. 1. Let

$$S_k := \{x_{j+k-2}, x_{j+k-1}, x_{j+k}\}, \quad k = 0, 1, 2 \tag{8}$$

be the sub-stencil consisting of 3 points starting at x_{j+k-2}. A third-order accurate quadratic polynomial approximation to the function $h(x)$ in Eq. (3) is constructed, i.e., $\hat{f}^k(x) = h(x) + O(\Delta x^3)$, with $k = 0, 1, 2$ for each of the three candidate stencils. These polynomial approximate functions are found to be (e.g., see [15])

Fig. 1 Candidate stencils used for the classic WENO5 numerical flux $\hat{f}_{j+1/2}$

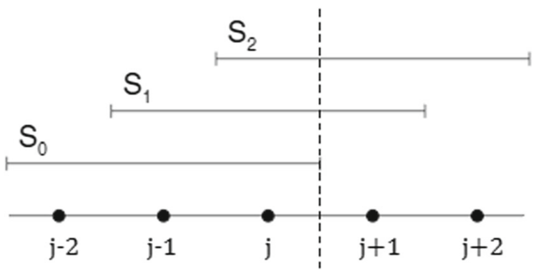

$$
\begin{aligned}
\hat{f}^0(x)&=\frac{-f_j+26f_{j-1}-f_{j-2}}{24}+\frac{f_j-f_{j-2}}{2\Delta x}(x-x_{j-1})+\frac{f_j-2f_{j-1}+f_{j-2}}{2\Delta x^2}(x-x_{j-1})^2,\\
\hat{f}^1(x)&=\frac{-f_{j+1}+26f_j-f_{j-1}}{24}+\frac{f_{j+1}-f_{j-1}}{2\Delta x}(x-x_j)+\frac{f_{j+1}-2f_j+f_{j-1}}{2\Delta x^2}(x-x_j)^2,\\
\hat{f}^2(x)&=\frac{-f_{j+2}+26f_{j+1}-f_j}{24}+\frac{f_{j+2}-f_j}{2\Delta x}(x-x_{j+1})+\frac{f_{j+2}-2f_{j+1}+f_j}{2\Delta x^2}(x-x_{j+1})^2.
\end{aligned}
\tag{9}
$$

Evaluations of Eq. (9) at the $j+1/2$ interface give $\hat{f}^k_{j+1/2}$ for each stencil:

$$
\begin{aligned}
\hat{f}^0_{j+\frac{1}{2}}&=\frac{1}{3}f_{j-2}-\frac{7}{6}f_{j-1}+\frac{11}{6}f_j,\\
\hat{f}^1_{j+\frac{1}{2}}&=-\frac{1}{6}f_{j-1}+\frac{5}{6}f_j+\frac{1}{3}f_{j+1},\\
\hat{f}^2_{j+\frac{1}{2}}&=\frac{1}{3}f_j+\frac{5}{6}f_{j+1}-\frac{1}{6}f_{j+2}.
\end{aligned}
\tag{10}
$$

The candidate numerical fluxes $\hat{f}^k_{j+1/2}$ $(k=0,1,2)$ are combined in a weighted average to define the fifth-order WENO approximation to the value $h(x_{j+1/2})$,

$$
\hat{f}_{j+\frac{1}{2}}=\sum_{k=0}^{2}\omega_k\hat{f}^k_{j+\frac{1}{2}},
\tag{11}
$$

where ω_k is the nonlinear weight of the stencil S_k. In the standard WENO-JS scheme, ω_k is calculated as

$$
\omega_k=\frac{\alpha_k}{\sum_{l=0}^{2}\alpha_l},\quad \alpha_k=\frac{d_k}{(\varepsilon+\beta_k)^2},\quad k=0,1,2,
\tag{12}
$$

where $d_0=\frac{1}{10}$, $d_1=\frac{6}{10}$ and $d_2=\frac{3}{10}$ are the ideal weights, $0<\varepsilon\ll 1$ is a small positive parameter to prevent the denominator becoming zero, and β_k is the smoothness indicator for the candidate numerical flux $\hat{f}^k_{j+1/2}$. The smoothness indicator β_k introduced by Jiang and Shu [4] is given by

$$
\beta_k=\sum_{l=1}^{2}\Delta x^{2l-1}\int_{x_{j-\frac{1}{2}}}^{x_{j+\frac{1}{2}}}\left(\frac{\mathrm{d}^l\hat{f}^k(x)}{\mathrm{d}x^l}\right)^2\mathrm{d}x,\quad k=0,1,2.
\tag{13}
$$

Equation (13) have the explicit expressions based on the polynomial approximations (9),

$$
\begin{aligned}
\beta_0&=\frac{1}{4}(f_{j-2}-4f_{j-1}+3f_j)^2+\frac{13}{12}(f_{j-2}-2f_{j-1}+f_j)^2,\\
\beta_1&=\frac{1}{4}(f_{j-1}-f_{j+1})^2+\frac{13}{12}(f_{j-1}-2f_j+f_{j+1})^2,\\
\beta_2&=\frac{1}{4}(3f_j-4f_{j+1}+f_{j+2})^2+\frac{13}{12}(f_j-2f_{j+1}+f_{j+2})^2.
\end{aligned}
\tag{14}
$$

Henrick et al. [5] noticed that by using the Taylor series expansions of the Eq. (10) and their counterparts at $j-1/2$, one can get

$$
\begin{aligned}
\hat{f}^0_{j\pm\frac{1}{2}}&=h_{j\pm\frac{1}{2}}-\frac{1}{4}f_j'''\Delta x^3+\mathrm{O}(\Delta x^4),\\
\hat{f}^1_{j\pm\frac{1}{2}}&=h_{j\pm\frac{1}{2}}+\frac{1}{12}f_j'''\Delta x^3+\mathrm{O}(\Delta x^4),\\
\hat{f}^2_{j\pm\frac{1}{2}}&=h_{j\pm\frac{1}{2}}-\frac{1}{12}f_j'''\Delta x^3+\mathrm{O}(\Delta x^4)
\end{aligned}
\tag{15}
$$

Denote $A_0 = -\frac{1}{4} f_j^{'''}$, $A_1 = \frac{1}{12} f_j^{'''}$, $A_2 = -\frac{1}{12} f_j^{'''}$ for the second terms in (15). Henrick et al. [5] derived the necessary and sufficient conditions on the weights for fifth-order convergence of a nominal fifth-order WENO scheme,

$$\begin{aligned}\sum_{k=0}^{2}(\omega_k^{\pm} - d_k) &= \mathrm{O}(\Delta x^6),\\ \sum_{k=0}^{2} A_k(\omega_k^{+} - \omega_k^{-}) &= \mathrm{O}(\Delta x^3),\\ \omega_k^{\pm} - d_k &= \mathrm{O}(\Delta x^2),\end{aligned} \tag{16}$$

where superscripts "+" and "−" on ω_k correspond to their use in $\hat{f}^k_{j+1/2}$ and $\hat{f}^k_{j-1/2}$ respectively. Since the first equation in (16) always holds due to the normalization, a simple sufficient condition for fifth-order convergence is give in [6] as

$$\omega_k^{\pm} - d_k = \mathrm{O}(\Delta x^3). \tag{17}$$

3 New Modified Fifth-Order WENO Scheme

In this section, we introduce high-order correction terms to the stencil approximation polynomials (9) to construct a new modified fifth-order WENO scheme, and analyze its order of accuracy.

3.1 Modified Stencil Approximation

We add cubic correction terms $p^k(x)$ to the candidate stencil polynomials (9),

$$\tilde{f}^k(x) = \hat{f}^k(x) + p^k(x), \quad k = 0, 1, 2. \tag{18}$$

We require that the modified polynomial $\tilde{f}^k(x)$ satisfy Eq. (3) at each grid point of the stencil S_k as shown in Fig. 1, and that it be a fourth-order accurate approximation to the function $h(x)$. The first constraint requires

$$f_i = \frac{1}{\Delta x}\int_{x_i-\frac{\Delta x}{2}}^{x_i+\frac{\Delta x}{2}} \tilde{f}^k(x)\mathrm{d}x, \quad i = j+k-2,\ j+k-1,\ j+k. \tag{19}$$

Because $\hat{f}^k(x)$ alone has already satisfied Eq. (19) [4,15], $p^k(x)$ should satisfy

$$\int_{x_i-\frac{\Delta x}{2}}^{x_i+\frac{\Delta x}{2}} p^k(x)\mathrm{d}x = 0, \quad i = j+k-2,\ j+k-1,\ j+k. \tag{20}$$

There are several choices for the form of $p^k(x)$ that can satisfy Eq. (20). In this paper, we choose

$$p^k(x) = a_k\left(x - x_{j+k-2}\right)^3 + b_k\left(x - x_{j+k-1}\right)^3 + c_k\left(x - x_{j+k}\right)^3, \quad k = 0, 1, 2. \tag{21}$$

Substituting (21) into (20), we obtain

$$5b_k + 34c_k = 0,\ a_k - c_k = 0,\ 34a_k + 5b_k = 0, \quad k = 0, 1, 2. \tag{22}$$

Thus, $a_k = c_k,\ b_k = -\frac{34}{5}c_k$. So, Eq. (21) becomes

$$p^k(x) = c_k\left[\left(x - x_{j+k-2}\right)^3 - \frac{34}{5}\left(x - x_{j+k-1}\right)^3 + \left(x - x_{j+k}\right)^3\right],\quad k = 0, 1, 2. \tag{23}$$

The second constraint requires that $\tilde{f}^k_{j+1/2}$ be a fourth-order accurate approximation to $h_{j+1/2}$, i.e, $\tilde{f}^k_{j+1/2} = \hat{f}^k_{j+1/2} + p^k(x_{j+1/2}) = h_{j+1/2} + \mathrm{O}(\Delta x^4)$, $k = 0, 1, 2$. By using Eq. (15), we obtain

$$\begin{aligned}
h_{j+\frac{1}{2}} - \frac{1}{4}f_j^{'''}\Delta x^3 + p^0\left(x_{j+\frac{1}{2}}\right) + \mathrm{O}(\Delta x^4) &= h_{j+\frac{1}{2}} + \mathrm{O}(\Delta x^4),\\
h_{j+\frac{1}{2}} + \frac{1}{12}f_j^{'''}\Delta x^3 + p^1\left(x_{j+\frac{1}{2}}\right) + \mathrm{O}(\Delta x^4) &= h_{j+\frac{1}{2}} + \mathrm{O}(\Delta x^4),\\
h_{j+\frac{1}{2}} - \frac{1}{12}f_j^{'''}\Delta x^3 + p^2\left(x_{j+\frac{1}{2}}\right) + \mathrm{O}(\Delta x^4) &= h_{j+\frac{1}{2}} + \mathrm{O}(\Delta x^4).
\end{aligned} \tag{24}$$

These equations give $c_k = -\frac{5}{144}f_j^{'''}$, $\forall k \in \{0, 1, 2\}$. Thus, $p^k(x)$ takes the specific form

$$p^k(x) = -\frac{5}{144}f_j^{'''}\left[\left(x - x_{j+k-2}\right)^3 - \frac{34}{5}\left(x - x_{j+k-1}\right)^3 + \left(x - x_{j+k}\right)^3\right], k = 0, 1, 2. \tag{25}$$

If we use a finite difference approximation for $f_j^{'''}$ in Eq. (25) as Ref. [12] did,

$$f_j^{'''} = \left.\frac{\partial^3 f}{\partial x^3}\right|_{x=x_j} \approx \frac{-f_{j-2} + 2f_{j-1} - 2f_{j+1} + f_{j+2}}{2\Delta x^3} + \mathrm{O}(\Delta x), \tag{26}$$

then $p^k(x)$ becomes

$$\begin{aligned}
p^k(x) = &-\frac{5}{288\Delta x^3}(-f_{j-2} + 2f_{j-1} - 2f_{j+1} + f_{j+2})\\
&\left[\left(x - x_{j+k-2}\right)^3 - \frac{34}{5}\left(x - x_{j+k-1}\right)^3 + \left(x - x_{j+k}\right)^3\right],\quad k = 0, 1, 2.
\end{aligned} \tag{27}$$

Obviously, the finite difference (26) will not degrade the fourth-order accuracy of $\tilde{f}^k(x)$ in approximating $h(x)$. Finally, evaluations of the modified stencil polynomials (18) with (27) at the grid interface $j + 1/2$ give the modified candidate fluxes as

$$\begin{aligned}
\tilde{f}^0_{j+\frac{1}{2}} &= \frac{1}{3}f_{j-2} - \frac{7}{6}f_{j-1} + \frac{11}{6}f_j \ + \frac{1}{8}\left(-f_{j-2} + 2f_{j-1} - 2f_{j+1} + f_{j+2}\right),\\
\tilde{f}^1_{j+\frac{1}{2}} &= -\frac{1}{6}f_{j-1} + \frac{5}{6}f_j + \frac{1}{3}f_{j+1} \ - \frac{1}{24}\left(-f_{j-2} + 2f_{j-1} - 2f_{j+1} + f_{j+2}\right),\\
\tilde{f}^2_{j+\frac{1}{2}} &= \frac{1}{3}f_j + \frac{5}{6}f_{j+1} - \frac{1}{6}f_{j+2} \ + \frac{1}{24}(-f_{j-2} + 2f_{j-1} - 2f_{j+1} + f_{j+2}).
\end{aligned} \tag{28}$$

We remark that the candidate numerical fluxes (28) are the same as those in the P-WENO scheme [12]. Nevertheless, the smoothness indicator and weights as described in the next subsection are different.

3.2 The New Smoothness Indicator and the WENO-MS Scheme

The Jiang-Shu smoothness indicator formula for the modified stencil polynomial approximations (18) can be written as

$$\tilde{\beta}_k = \sum_{l=1}^{3} \Delta x^{2l-1} \int_{x_{j-\frac{1}{2}}}^{x_{j+\frac{1}{2}}} \left\{ \frac{\mathrm{d}^l}{\mathrm{d}x^l} \left[\hat{f}^k(x) + p^k(x) \right] \right\}^2 \mathrm{d}x. \tag{29}$$

After integration, the modified indicators take on explicit forms:

$$\begin{aligned}
\tilde{\beta}_0 &= \beta_0 + \frac{547}{960}(-f_{j-2} + 2f_{j-1} - 2f_{j+1} + f_{j+2})^2 \\
&\quad + \frac{1}{12}(-f_{j-2} + 2f_{j-1} - 2f_{j+1} + f_{j+2})(15f_{j-2} - 34f_{j-1} + 19f_j), \\
\tilde{\beta}_1 &= \beta_1 + \frac{89}{320}(-f_{j-2} + 2f_{j-1} - 2f_{j+1} + f_{j+2})^2 \\
&\quad - \frac{1}{12}(-f_{j-2} + 2f_{j-1} - 2f_{j+1} + f_{j+2})(f_{j+1} - f_{j-1}), \\
\tilde{\beta}_2 &= \beta_2 + \frac{547}{960}(-f_{j-2} + 2f_{j-1} - 2f_{j+1} + f_{j+2})^2 \\
&\quad - \frac{1}{12}(-f_{j-2} + 2f_{j-1} - 2f_{j+1} + f_{j+2})(19f_j - 34f_{j+1} + 15f_{j+2}).
\end{aligned} \tag{30}$$

The nonlinear weights ω_k are calculated as the WENO-JS scheme,

$$\omega_k = \frac{\alpha_k}{\sum_{l=0}^{2} \alpha_l}, \quad \alpha_k = \frac{d_k}{\left(\varepsilon + \tilde{\beta}_k\right)^2}, \quad k = 0, 1, 2. \tag{31}$$

where $\varepsilon = 10^{-40}$ is used in the present scheme. It is easy to see that the ideal weights $d_0 = \frac{1}{10}$, $d_1 = \frac{6}{10}$ and $d_2 = \frac{3}{10}$ also make the linear combination of the modified candidate fluxes (28) have the optimal fifth-order accuracy, i.e.,

$$\begin{aligned}
\sum_{k=0}^{2} d_k \tilde{f}^k_{j+\frac{1}{2}} &= \frac{1}{60}(2f_{j-2} - 13f_{j-1} + 47f_j + 27f_{j+1} - 3f_{j+2}) \\
&= h_{j+1/2} + \mathrm{O}(\Delta x^5).
\end{aligned} \tag{32}$$

Based on the modified candidate fluxes (28) and smoothness indicators (30), as well as the nonlinear weights (31), a naive weighted scheme is given by

$$\tilde{f}^{\mathrm{MS}}_{j+\frac{1}{2}} = \sum_{k=0}^{2} \omega_k \tilde{f}^k_{j+\frac{1}{2}}, \tag{33}$$

where “MS” stands for “modified stencil”.

However, the modified candidate fluxes (28) and smoothness indicators (30) depend on the whole 5-point stencil thus the naive scheme (33) loses the ENO property. Ref. [12] retained the WENO-JS smoothness indicators and applied a tunable function φ to limit the influence of the last terms in Eq. (28) to recover the ENO property. In this work, we multiply the last terms in Eq. (28) and the last two terms in Eq. (30) by using a tunable function φ in order to recover the ENO property. The smoothness indicators (30) become

$$
\begin{aligned}
\tilde{\tilde{\beta}}_0 &= \beta_0 + \varphi \left(\frac{547}{960} \left(-f_{j-2} + 2f_{j-1} - 2f_{j+1} + f_{j+2} \right)^2 \right. \\
&\quad \left. + \frac{1}{12} \left(-f_{j-2} + 2f_{j-1} - 2f_{j+1} + f_{j+2} \right) \left(15f_{j-2} - 34f_{j-1} + 19f_j \right) \right), \\
\tilde{\tilde{\beta}}_1 &= \beta_1 + \varphi \left(\frac{89}{320} \left(-f_{j-2} + 2f_{j-1} - 2f_{j+1} + f_{j+2} \right)^2 \right. \\
&\quad \left. - \frac{1}{12} \left(-f_{j-2} + 2f_{j-1} - 2f_{j+1} + f_{j+2} \right) \left(f_{j+1} - f_{j-1} \right) \right), \\
\tilde{\tilde{\beta}}_2 &= \beta_2 + \varphi \left(\frac{547}{960} \left(-f_{j-2} + 2f_{j-1} - 2f_{j+1} + f_{j+2} \right)^2 \right. \\
&\quad \left. - \frac{1}{12} \left(-f_{j-2} + 2f_{j-1} - 2f_{j+1} + f_{j+2} \right) \left(19f_j - 34f_{j+1} + 15f_{j+2} \right) \right),
\end{aligned} \tag{34}
$$

where φ is defined as

$$\varphi = 1 - \left(\frac{|\beta_0 - \beta_2|}{\beta_0 + \beta_2 + \varepsilon} \right)^q, \quad q \geq 1. \tag{35}$$

And the candidate fluxes (28) become $\tilde{\tilde{f}}^k_{j+1/2}$ similarly. We call Eq. (33) with the φ-limited candidate fluxes $\tilde{\tilde{f}}^k_{j+1/2}$ and smoothness indicators $\tilde{\tilde{\beta}}_k$ the WENO-MS scheme.

From Eq. (35) we can see that if any of the three candidate stencils in Fig. 1 contains a discontinuity, then φ is a small value approaching zero. Thus $\tilde{\tilde{\beta}}_k \to \beta_k$, $\tilde{\tilde{f}}^k_{j+1/2} \to \hat{f}^k_{j+1/2}$, $\forall k = 0, 1, 2$ so that WENO-MS recovers WENO-JS; otherwise, $\varphi = 1 - \left(\frac{\mathrm{O}(\Delta x^5)}{\mathrm{O}(\Delta x^2)}\right)^q = 1 - \mathrm{O}(\Delta x^{3q})$ for $f'_j \neq 0$, and $\varphi = 1 - \left(\frac{\mathrm{O}(\Delta x^5)}{\mathrm{O}(\Delta x^4)}\right)^q = 1 - \mathrm{O}(\Delta x^q)$ for $f'_j = 0$ [12]. We take $q = 1$. Such a φ does not affect the fifth-order convergence of the scheme (33) in smooth regions as will be shown in Sect. 3.3.

3.3 Accuracy Analysis of the WENO-MS Scheme

In smooth region of solution, Taylor series expansions of the smoothness indicators (30) at x_j give

$$
\begin{aligned}
\tilde{\beta}_0 &= f_j'^2 \Delta x^2 + \frac{13}{12} f_j''^2 \Delta x^4 + \frac{1}{2} f_j' f_j^{(4)} \Delta x^5 + \mathrm{O}(\Delta x^6), \\
\tilde{\beta}_1 &= f_j'^2 \Delta x^2 + \frac{13}{12} f_j''^2 \Delta x^4 + \mathrm{O}(\Delta x^6), \\
\tilde{\beta}_2 &= f_j'^2 \Delta x^2 + \frac{13}{12} f_j''^2 \Delta x^4 - \frac{1}{2} f_j' f_j^{(4)} \Delta x^5 + \mathrm{O}(\Delta x^6).
\end{aligned} \tag{36}
$$

Taylor series expansions of Eq. (34) also give the same results as long as $\varphi = 1 + \mathrm{O}(\Delta x)$, since the affected last two terms in Eq. (34) contain only $\mathrm{O}(\Delta x^5)$. Similar to the analysis made in Ref. [5], Eq. (36) can be written as

$$\tilde{\beta}_k = D \left(1 + \mathrm{O}(\Delta x^2) \right). \tag{37}$$

where $D = f_j'^2 \Delta x^2$ if $f'_j \neq 0$, $f''_j \neq 0$ and $D = \frac{12}{13} f_j''^2 \Delta x^4$ if $f'_j = 0$, $f''_j \neq 0$. Notice that (37) is different from $\beta_k = D\,(1 + \mathrm{O}(\Delta x))$ for $f'_j = 0$ in Refs. [5,9,12]. Substitution of Eq. (37) into the second equation of the weights (31) gives

$$\alpha_k = \frac{d_k}{\left(D\left(1+\mathrm{O}(\Delta x^2)\right)\right)^2} = \frac{d_k}{D^2}\left(1+\mathrm{O}(\Delta x^2)\right). \tag{38}$$

In view of $\sum_{k=0}^{2} d_k = 1$, the sum of these terms is

$$\sum_{k=0}^{2} \alpha_k = \frac{1}{D^2}\left(1+\mathrm{O}(\Delta x^2)\right). \tag{39}$$

Thus the weights (31) satisfy the following relation:

$$\omega_k = d_k + \mathrm{O}(\Delta x^2). \tag{40}$$

Now, we derive the necessary and sufficient conditions for fifth-order convergence of the WENO-MS scheme. We add and subtract $\sum_{k=0}^{2} d_k \tilde{f}^k_{j+1/2}$ from Eq. (33):

$$\begin{aligned} \hat{f}^{\mathrm{MS}}_{j+\frac{1}{2}} &= \sum_{k=0}^{2} d_k \tilde{f}^k_{j+\frac{1}{2}} + \sum_{k=0}^{2} (\omega^+_k - d_k)\tilde{f}^k_{j+\frac{1}{2}}, \\ \hat{f}^{\mathrm{MS}}_{j-\frac{1}{2}} &= \sum_{k=0}^{2} d_k \tilde{f}^k_{j-\frac{1}{2}} + \sum_{k=0}^{2} (\omega^-_k - d_k)\tilde{f}^k_{j-\frac{1}{2}}. \end{aligned} \tag{41}$$

The numerical flux difference $\hat{f}^{\mathrm{MS}}_{j+1/2} - \hat{f}^{\mathrm{MS}}_{j-1/2}$ can be expanded as

$$\begin{aligned} &\sum_{k=0}^{2} \omega^+_k \tilde{f}^k_{j+1/2} - \sum_{k=0}^{2} \omega^-_k \tilde{f}^k_{j-1/2} \\ &= \underbrace{\sum_{k=0}^{2} d_k \tilde{f}^k_{j+1/2} - \sum_{k=0}^{2} d_k \tilde{f}^k_{j-1/2}}_{\text{linear flux difference}} + \sum_{k=0}^{2} (\omega^+_k - d_k)\tilde{f}^k_{j+1/2} \ - \sum_{k=0}^{2} (\omega^-_k - d_k)\tilde{f}^k_{j-1/2} \\ &= \underbrace{h_{j+\frac{1}{2}} - \frac{1}{60}\left.\frac{\mathrm{d}^5 f}{\mathrm{d}x^5}\right|_j \Delta x^5 - h_{j-\frac{1}{2}} + \frac{1}{60}\left.\frac{\mathrm{d}^5 f}{\mathrm{d}x^5}\right|_j \Delta x^5 + \mathrm{O}(\Delta x^6)}_{\text{linear flux difference}} \\ &\quad + \sum_{k=0}^{2} (\omega^+_k - d_k)\underbrace{\left(h_{j+\frac{1}{2}} + A_k \Delta x^4 + \mathrm{O}(\Delta x^5)\right)}_{=\tilde{f}^k_{j+1/2},\ k=0,1,2} - \sum_{k=0}^{2} (\omega^-_k - d_k)\underbrace{\left(h_{j-\frac{1}{2}} + A_k \Delta x^4 + \mathrm{O}(\Delta x^5)\right)}_{=\tilde{f}^k_{j-1/2},\ k=0,1,2} \\ &= \underbrace{f'_j \Delta x + \mathrm{O}(\Delta x^6)}_{\text{linear scheme}} + \Delta x^4 \sum_{k=0}^{2} \left(\omega^+_k - \omega^-_k\right) A_k + \left[\sum_{k=0}^{2} (\omega^+_k - d_k) - \sum_{k=0}^{2} (\omega^-_k - d_k)\right] \mathrm{O}(\Delta x^5), \end{aligned}$$

where the normalization has been utilized for the last equality. (In fact, $\tilde{\tilde{f}}^k_{j\pm1/2} = h_{j\pm1/2} + \mathrm{O}(\Delta x^4)$ is also valid as long as $\varphi = 1 + \mathrm{O}(\Delta x)$ because the last terms in Eq. (28) contain only $\mathrm{O}(\Delta x^3)$). The last two terms give the necessary and sufficient conditions

$$\sum_{k=0}^{2} \left(\omega^+_k - \omega^-_k\right) A_k = \mathrm{O}(\Delta x^2), \tag{42a}$$

$$\omega^\pm_k - d_k = \mathrm{O}(\Delta x). \tag{42b}$$

It is only sufficient to require $\omega_k - d_k = O(\Delta x^2)$, i.e., Eq. (40). This sufficient condition relaxes the original requirement on the weights (Eq. (17)) by one order. We remark that the condition was also derived in the P-WENO scheme [12] in a slightly different way.

Since the nonlinear weights (31) always satisfy the condition (40) whether $f_j^{'} = 0$ or $f_j^{'} \neq 0$, we conclude that the proposed WENO-MS scheme is fifth-order accurate in smooth regions including first-order critical points.

4 Numerical Results

In this section, we demonstrate the performance of the proposed WENO-MS scheme in several numerical examples in comparison with the WENO-JS, WENO-M, WENO-Z and P-WENO schemes. The numerical examples begin with solutions of the simple scalar advection equation, followed by numerical solutions of the one-dimensional and two-dimensional Euler equations. The local Lax–Friedrichs flux splitting is used for all schemes and examples in this paper. For the time advancement we use the third-order TVD Runge–Kutta method [13].

4.1 One-Dimensional Scalar Advection Problems

Consider the following linear advection equation:

$$u_t + u_x = 0, \quad -1 \leq x \leq 1, \quad t \geq 0 \tag{43}$$

with the initial condition $u(x, 0) = u_0(x)$ and periodic boundary conditions.

Firstly, we test the approximation order of the WENO-MS scheme on Eq. (43) with two sets of initial data (e.g., [7,12])

$$\text{(a) } u_0(x) = \sin(\pi x), \quad \text{(b) } u_0(x) = \sin\left(\pi x - \frac{\sin(\pi x)}{\pi}\right). \tag{44}$$

Since we use the third-order TVD Runge–Kutta method in time, the time step is taken as $\Delta t = 0.5 \times (\Delta x)^{5/3}$ such that it becomes effectively fifth-order. Table 1 gives the L^∞ errors and convergence orders with increasing node number N at $t = 2$ for the initial data (44a). This initial data have no first-order critical points. It can be seen that the errors of the WENO-MS scheme are close to those of the WENO-M, WENO-Z, and P-WENO schemes. Table 2 shows results for the initial data (44b). It is seen that the present scheme has smaller or comparable errors than other improved WENO schemes for this case with first-order critical points.

Table 3 shows the local errors and rates of convergence of the four schemes at the first-order critical point $x_c \approx 0.59$ for the initial condition (44b). We can see that WENO-MS, WENO-M and P-WENO attain fifth-order, while WENO-Z attains fourth-order and WENO-JS attains third-order accuracy, respectively.

To compare the computational costs, Table 4 shows the CPU times of different schemes spent in doing 1000 WENO reconstructions. We see that the CPU costs of the WENO-M, WENO-Z, P-WENO, and WENO-MS schemes increase roughly 33%, 1%, 3%, and 7% compared with the classical WENO-JS scheme, respectively.

Secondly, we check the behaviors of the present scheme at jump discontinuities after a long time by using the following three cases. In the first case, we test it on the linear advection Eq. (43) with the initial condition [8]

$$u_0(x) = \begin{cases} -\sin(\pi x) - \frac{1}{2}x^3, & \text{if } -1 \leq x \leq 0, \\ -\sin(\pi x) - \frac{1}{2}x^3 + 1, & \text{if } 0 \leq x \leq 1, \end{cases} \tag{45}$$

Table 1 L^∞ errors and convergence orders at $t = 2.0$ of different schemes on the linear advection equation (43) with the initial condition (44a)

N	WENO-JS L^∞ error (order)	WENO-M L^∞ error (order)	WENO-Z L^∞ error (order)	P-WENO L^∞ error (order)	WENO-MS L^∞ error (order)
10	4.76E−2 (—)	1.33E−2 (—)	1.04E−2 (—)	1.16E−2 (—)	1.38E−2 (—)
20	2.54E−3 (4.23)	3.34E−4 (5.31)	3.33E−4 (4.96)	3.42E−4 (5.08)	4.02E−4 (5.10)
40	8.03E−5 (4.98)	9.87E−6 (5.08)	1.03E−5 (5.01)	9.37E−6 (5.19)	1.12E−5 (5.17)
80	2.43E−6 (5.04)	2.36E−7 (5.39)	2.96E−7 (5.12)	2.64E−7 (5.15)	3.04E−7 (5.20)
160	8.08E−8 (4.91)	7.36E−9 (5.00)	7.71E−9 (5.26)	7.36E−9 (5.16)	8.57E−9 (5.15)
320	2.46E−9 (5.04)	1.96E−10 (5.23)	2.36E−10 (5.03)	2.23E−10 (5.04)	2.58E−10 (5.05)

WENO-JS uses $\varepsilon = 10^{-6}$ while other schemes use $\varepsilon = 10^{-40}$

Table 2 L^∞ errors and convergence orders at $t = 2.0$ of different schemes on the linear advection equation (43) with the initial condition (44b)

N	WENO-JS L^∞ error (order)	WENO-M L^∞ error (order)	WENO-Z L^∞ error (order)	P-WENO L^∞ error (order)	WENO-MS L^∞ error (order)
10	1.23E−1 (—)	7.36E−2 (—)	5.21E−2 (—)	4.38E−2 (—)	4.63E−2 (—)
20	1.43E−2 (3.10)	5.26E−3 (3.81)	3.50E−3 (3.89)	1.87E−3 (4.55)	1.77E−3 (4.71)
40	1.10E−3 (3.68)	2.09E−4 (4.66)	1.21E−4 (4.86)	6.13E−5 (4.93)	5.51E−5 (5.01)
80	4.27E−5 (4.69)	4.58E−6 (5.51)	2.58E−6 (5.55)	1.53E−6 (5.32)	1.48E−6 (5.22)
160	1.30E−6 (5.04)	1.31E−7 (5.13)	6.71E−8 (5.27)	3.81E−08 (5.33)	4.12E−8 (5.17)
320	4.03E−8 (5.01)	4.09E−8 (5.00)	2.10E−9 (5.00)	1.14E−09 (5.06)	1.27E−9 (5.02)

Table 3 The point errors $|u - u_{\text{exact}}|$ at the critical point $x_c \approx 0.59$ and corresponding convergence orders at $t = 2.0$ of different schemes on the linear advection equation (43) with the initial condition (44b)

N	WENO-JS L^∞-error (order)	WENO-M L^∞-error (order)	WENO-Z L^∞-error (order)	P-WENO L^∞-error (order)	WENO-MS L^∞-error (order)
20	1.60E−3(—)	2.53E−4(—)	2.90E−4(—)	2.36E−4(—)	2.65E−4(—)
40	2.34E−4 (2.77)	7.96E−6 (4.99)	2.14E−5 (3.87)	7.81E−6 (4.92)	8.46E−6 (4.97)
80	3.05E−5 (2.93)	2.53E−7 (4.98)	1.37E−6 (3.96)	2.47E−7 (4.98)	2.67E−7 (4.99)
160	4.10E−6 (2.90)	7.94E−9 (4.99)	8.69E−8 (3.98)	7.76E−9 (4.99)	8.40E−9 (4.99)
320	5.31E−7 (2.95)	2.55E−10 (4.96)	5.46E−9 (3.99)	2.44E−10 (4.99)	2.65E−10 (4.99)

Table 4 CPU times in seconds and costs relative to the WENO-JS scheme for different schemes spent in doing 1000 WENO reconstructions for the linear advection equation (43) with the initial condition (44a)

N	WENO-JS	WENO-M	WENO-Z	P-WENO	WENO-MS
40	0.044 (1.00)	0.055 (1.25)	0.043 (0.98)	0.0452 (1.03)	0.0465 (1.06)
160	0.204 (1.00)	0.272 (1.33)	0.208 (1.02)	0.211 (1.03)	0.215 (1.05)
640	6.689 (1.00)	9.552 (1.43)	6.744 (1.01)	6.920 (1.03)	7.180 (1.07)

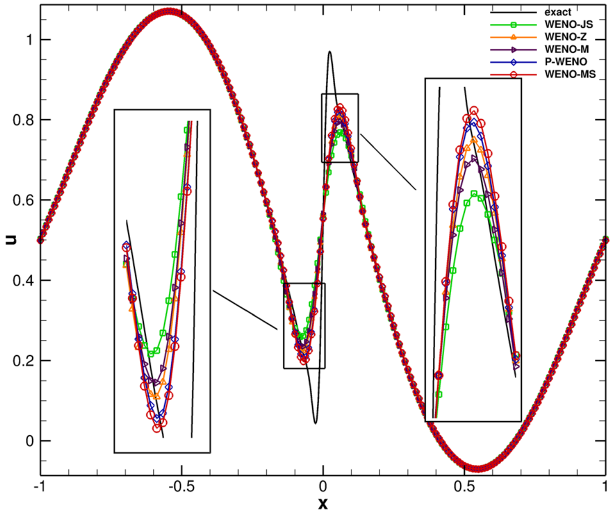

Fig. 2 Comparison of the analytical solution and the numerical solutions using WENO-JS, WENO-M, WENO-Z, P-WENO and WENO-MS schemes for the linear advection Eq. (43) with the initial condition (45) at $t = 40$, $\Delta x = 0.01$

Table 5 Local L^1 errors in the region [-0.15, 0.15] (near discontinuity) at $t = 40$ of different schemes for the linear advection Eq. (43) with the initial condition (45)

N	WENO-JS	WENO-M	WENO-Z	P-WENO	WENO-MS
50	4.0432E−02	3.5678E−02	3.6704E−02	3.5596E−02	3.5617E−02
100	2.6695E−02	2.3034E−02	2.3264E−02	2.2916E−02	2.3289E−02
200	1.6556E−02	1.4419E−02	1.4170E−02	1.4523E−02	1.4931E−02
400	9.6786E−03	8.5651E−03	8.3847E−03	8.6717E−03	9.0301E−03
800	5.2363E−03	4.5529E−03	4.5265E−03	4.6188E−03	4.7520E−03

which is a piecewise sine function with a jump discontinuity at $x = 0$. Numerical solutions of different schemes are compared with the analytic solution at $t = 40$ in Fig. 2. We can see that there are significant improvements near discontinuities with the WENO-MS and P-WENO schemes. Table 5 shows the L^1 errors near the discontinuity. We see that the results of WENO-MS, P-WENO, WENO-M and WENO-Z are comparable, all of which are slightly smaller than those of the WENO-JS scheme.

In the second case, the initial condition is [7,8]

$$u_0(x) = \begin{cases} -x \sin\left(\frac{3\pi}{2}x^2\right), & \text{if } -1 \le x \le -\frac{1}{3}, \\ |\sin(2\pi x)|, & \text{if } -\frac{1}{3} < x \le \frac{1}{3}, \\ 2x - 1 - \frac{1}{6}\sin(3\pi x), & \text{if } \frac{1}{3} \le x \le 1. \end{cases} \tag{46}$$

We solve the advection equation (43) with the initial condition (46) up to $t = 41$ with the CFL number of 0.5. The solution consists of contact discontinuities, corner singularities and smooth areas. The numerical results in Fig. 3, especially near the areas of discontinuities, show that WENO-MS performs slightly better than P-WENO, and both are better than WENO-Z, WENO-M, and WENO-JS.

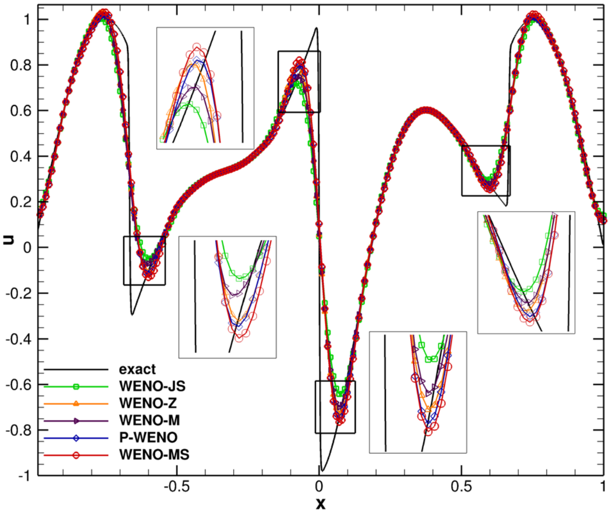

Fig. 3 Comparison of the analytical solution and the numerical solutions using WENO-JS, WENO-M, WENO-Z, P-WENO and WENO-MS schemes for the linear advection equation (43) with the initial condition (46) at $t = 41$, $\Delta x = 0.01$

In the third case, the initial condition containing a Gaussian, a square-wave, a triangle and a semi-ellipse wave, is given by [12]

$$u_0(x) = \begin{cases} \frac{1}{6}\left(G(x,\beta,z-\delta) + G(x,\beta,z+\delta) + 4G(x,\beta,z)\right), & \text{if } -0.8 \le x \le -0.6, \\ 1, & \text{if } -0.4 \le x \le -0.2, \\ 1 - |10(x-0.1)|, & \text{if } 0.0 < x \le 0.2, \\ \frac{1}{6}\left(F(x,\alpha,a-\delta) + G(x,\alpha,a+\delta) + 4G(x,\alpha,a)\right), & \text{if } 0.4 \le x \le 0.6, \\ 0, & \text{otherwise.} \end{cases} \tag{47}$$

where $G(x, \beta, z) = \exp^{-\beta(x-z)^2}$, $F(x, \alpha, a) = \sqrt{\max(1 - \alpha^2(x - a)^2, 0)}$, $a = 0.5$, $z = -0.7$, $\delta = 0.005$, $\alpha = 10$ and $\beta = \log 2/36\delta^2$. We solve the advection equation (43) with the condition (47) up to $t = 6$ using CFL $= 0.5$ and $\Delta x = 0.005$. The numerical results are shown in Fig. 4. Form the enlarged subsets we see that the present WENO-MS scheme is closer to the analytical solution than P-WENO, WENO-Z, WENO-M and WENO-JS. The present scheme is most close to the exact solution near the smooth peaks, while the WENO-JS scheme is more dissipative than other improved WENO schemes, both at smooth peaks and at discontinuities.

4.2 1D Euler Systems

We consider the system of the one-dimensional Euler equations,

$$U_t + F(U)_x = 0, \tag{48}$$

where

$$U = (\rho, \rho u, E)^T, \quad F(U) = \left(\rho u, \rho u^2 + p, u(E + p)\right)^T.$$

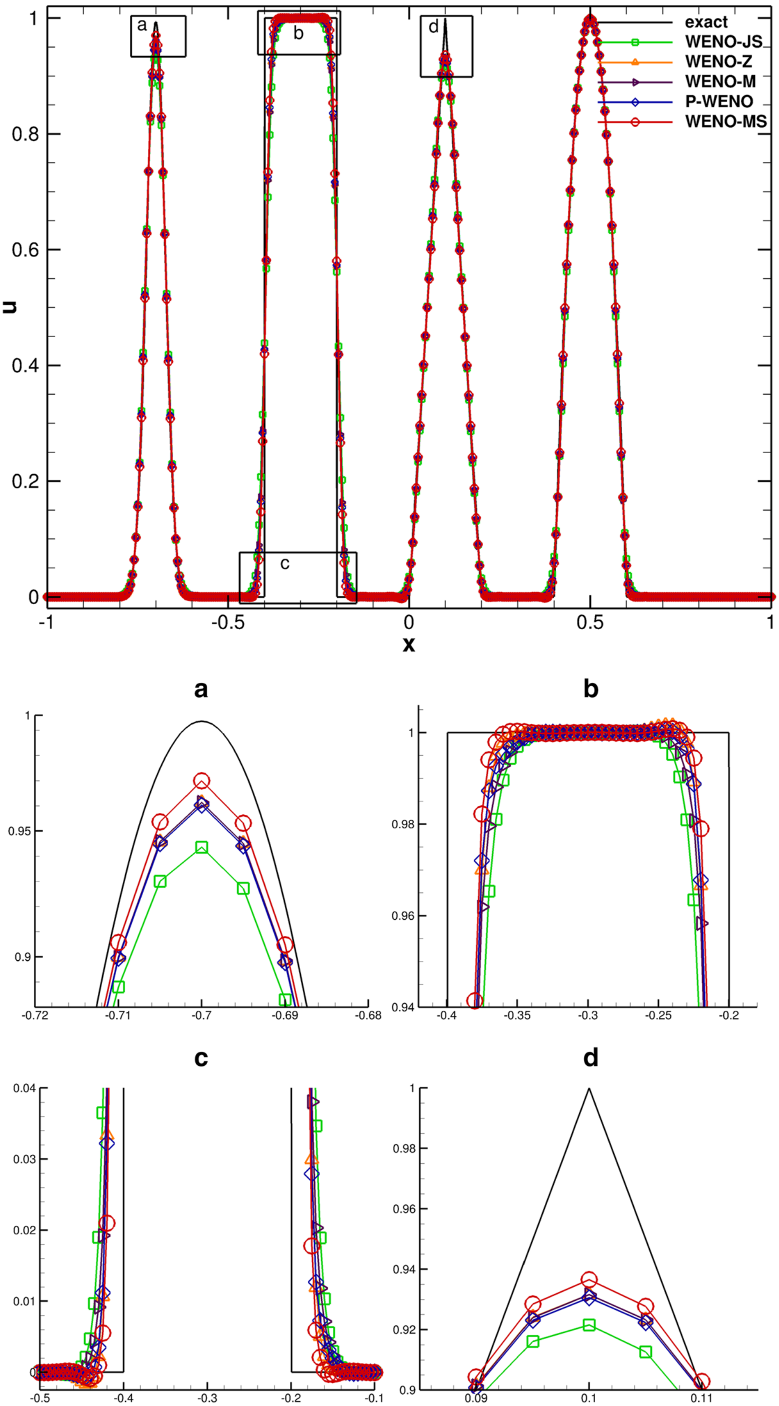

Fig. 4 Comparison between the analytical solution and the numerical solutions using WENO-JS, WENO-M, WENO-Z, P-WENO and WENO-MS schemes for the linear advection equation (43) with the initial condition (47) at $t = 6$, $\Delta x = 0.005$

The ideal gas equation of state is given by

$$p = (\gamma - 1)\left(E - \frac{1}{2}\rho u^2\right),$$

where ρ, u, p and E are the density, velocity, pressure and total energy respectively, γ is the ratio of specific heats, and $\gamma = 1.4$ is used throughout in this subsection. The characteristic decomposition [15] is used to generalize the WENO schemes to the 1D Euler system. We consider three examples. The CFL number used is set to 0.5 in all the examples.

1. Shock Entropy Wave Interaction (Shu–Osher Problem [13]**)** The solution domain is $x \in [-5, 5]$ with zero-gradient boundary conditions. The initial conditions are

$$(\rho, u, p) = \begin{cases} \left(\frac{27}{7}, \frac{4\sqrt{35}}{9}, \frac{31}{3}\right), & \text{if } -5 \le x < -4, \\ (1 + \varepsilon \sin(kx), 0, 1), & \text{if } -4 \le x \le 5, \end{cases} \tag{49}$$

where $\varepsilon = 0.2$ and $k = 5$ are the amplitude and wave number of the entropy wave, respectively. A right-going Mach 3 shock wave initially at $x = -4$ interacts with sine waves in a density disturbance which generates a flow field with both smooth structures and discontinuities. This flow induces high-frequency wave trails behind the main shock that are progressing into smaller amplitude shocks. Since the exact solution is unknown, the reference solution is obtained by using the fifth-order WENO-JS scheme [4] with 3201 grid points. The problem is solved with $\Delta x = 0.05$ and with $\Delta x = 0.025$ respectively. Figure 5 shows comparison between the numerical results of density profiles for different schemes and the exact solution at $t = 1.8$. It is seen that the present WENO-MS scheme captures the shock and the high-frequency waves better than other WENO schemes.

2. Sod's Shock Tube Problem [16,17] The initial conditions of this problem are given by

$$(\rho, u, p) = \begin{cases} (1.000, 0.0, 1.0), & \text{if } 0 \le x < 0.5, \\ (0.125, 0.0, 0.1), & \text{if } 0.5 \le x \le 1. \end{cases} \tag{50}$$

The computational domain is $x \in [0, 1]$ with zero-gradient boundary conditions. We solve the 1D Euler equations with the initial conditions (50) up to $t = 0.2$ with $\Delta x = 0.005$. The numerical results of the density distribution are displayed in Fig. 6. We see the present WENO-MS scheme has a resolution slightly higher than the P-WENO, WENO-Z, WENO-M, and WENO-JS schemes. We found that the use of the function φ (35) in the WENO-MS scheme can suppress spurious overshoots and undershoots at the contact discontinuity and the left end of the rarefaction wave.

3. Interacting Blast Waves [18] The initial conditions are given by

$$(\rho, u, p) = \begin{cases} (1,\ 0,\ 1000), & \text{if } 0.0 \le x < 0.1, \\ (1,\ 0,\ 0.01), & \text{if } 0.1 \le x < 0.9, \\ (1,\ 0,\ 100), & \text{if } 0.9 \le x \le 1.0 \end{cases} \tag{51}$$

with reflection boundary conditions at two ends. The initial pressure jumps generate two interacting shock waves. This problem is usually used to test the robustness and the capability of shock-capturing schemes. We solve the equation up to $t = 0.038$ with $\Delta x = 0.005$. The numerical results of the density and pressure field are displayed in Fig. 7. It is seen that WENO-MS performs better than the P-WENO, WENO-Z, WENO-M and WENO-JS schemes.

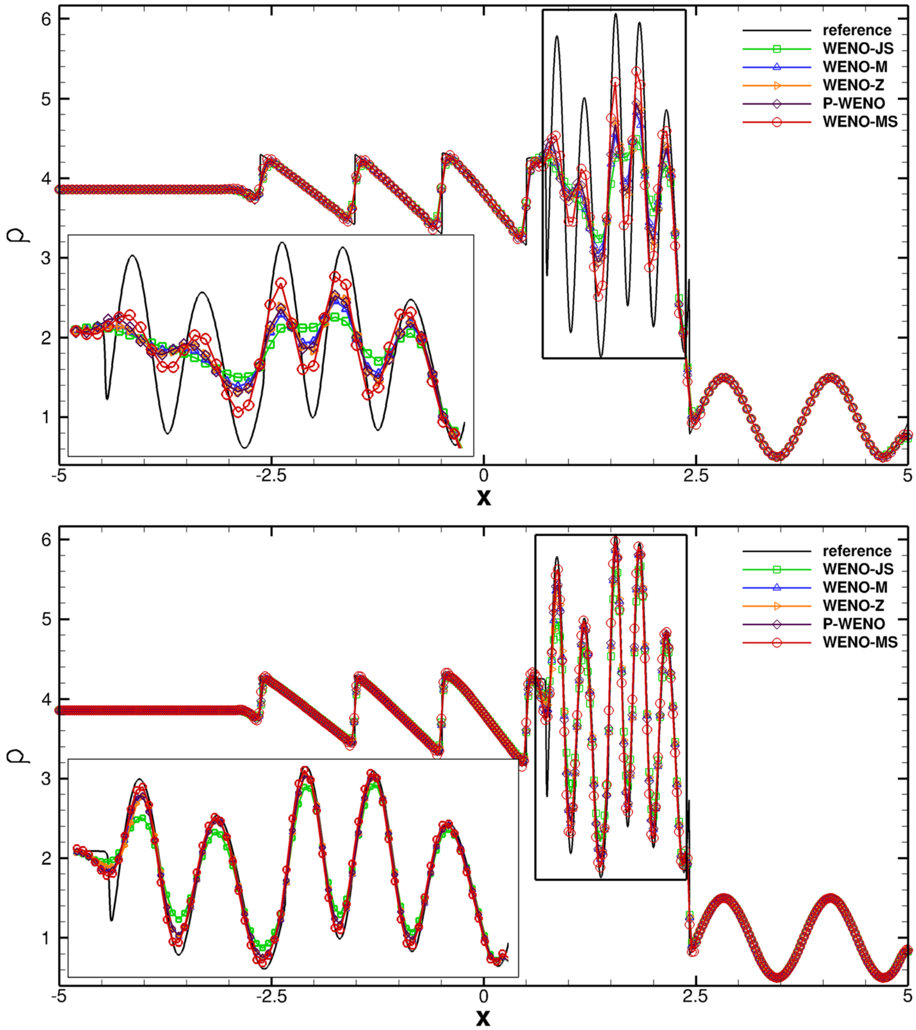

Fig. 5 Density profiles of the shock entropy wave interaction problem [13] computed using WENO-JS, WENO-M, WENO-Z, P-WENO and WENO-MS at $t = 1.8$ with a grid of $N = 200$ (top) and $N = 400$ (bottom)

4.3 2D Euler Systems

In this subsection we use the WENO-S scheme to solve the 2D compressible Euler equations,

$$U_t + F(U)_x + G(U)_y = 0, \tag{52}$$

where

$$\begin{aligned} U &= (\rho, \rho u, \rho v, E)^T, \\ F(U) &= (\rho u, p + \rho u^2, \rho u v, u(E+p))^T, \\ G(U) &= (\rho v, \rho v u, p + \rho v^2, v(E+p))^T. \end{aligned}$$

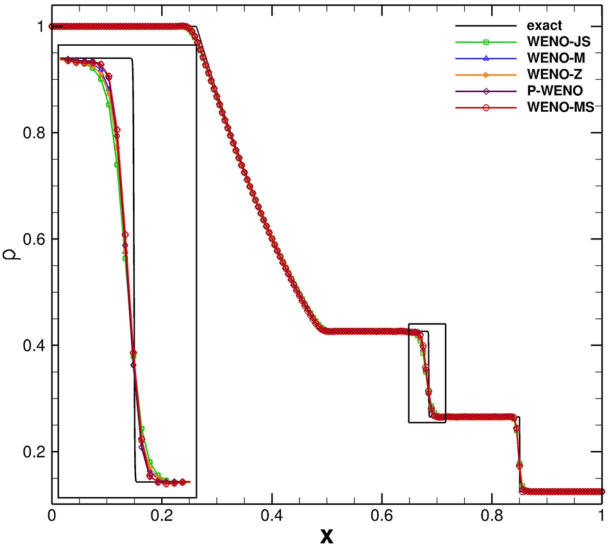

Fig. 6 Numerical results of the Sod problem [17] with WENO-JS, WENO-M, WENO-Z, P-WENO and WENO-MS schemes at $t = 0.2$, $N = 200$. Enlarged zone shows plot of the contact discontinuity

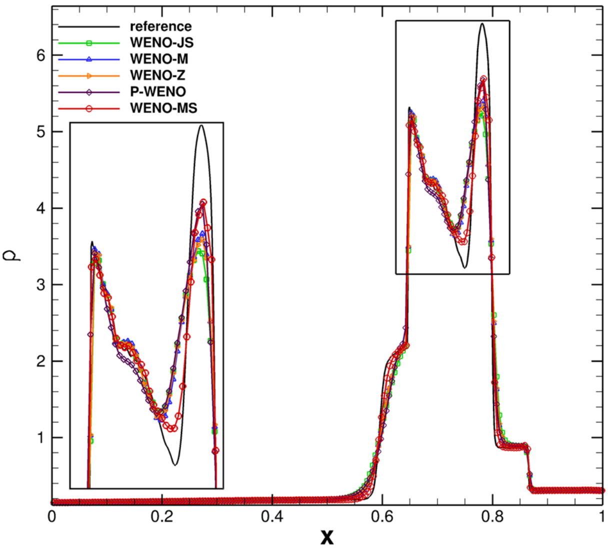

Fig. 7 Density profiles of interacting blast wave problem computed with WENO-JS, WENO-M, WENO-Z, P-WENO and WENO-MS schemes at $t = 0.038$, $N = 200$. Enlarged view show the three contact waves. Here "reference" solution is obtained by WENO-JS on 3200 points

The equation of state is given by

$$p = (\gamma - 1)\left(E - \frac{1}{2}\rho(u^2 + v^2)\right).$$

Here u, v are the velocity components in the x and y directions, respectively. The 2D Euler equations are solved in a dimension-by-dimension fashion. The Lax–Fridriches flux splitting is used. The time step is taken as Refs. [12,19] based a CFL number of 0.5 throughout all the examples.

1. 2D Riemann Problem [20] We solve this problem on the square domain $[0, 1] \times [0, 1]$. The 2D Riemann problem is defined by four initial constant states in the four quadrants divided by lines $x = 0.8$ and $y = 0.8$:

$$(\rho, u, v, p) = \begin{cases} (1.5,\ 0.0,\ 0.0,\ 1.5), & 0.8 \le x \le 1.0, 0.8 \le y \le 1.0, \\ (0.5323,\ 1.206,\ 0.0,\ 0.3), & 0.0 \le x < 0.8, 0.8 \le y \le 1.0, \\ (0.1380,\ 1.206,\ 1.206,\ 0.029), & 0.0 \le x < 0.8, 0.0 \le y < 0.8, \\ (0.5323,\ 1.206,\ 0.0,\ 0.3), & 0.8 < x \le 1.0, 0.0 \le y < 0.8. \end{cases} \tag{53}$$

The ratio of specific heats is taken as $\gamma = 1.4$. The numerical results at $t = 0.8$ with various WENO schemes are shown in Fig. 8 on 400×400 cells and in Fig. 9 on 800×800 cells. Careful comparison between these frames of each figure reveals that WENO-MS and P-WENO produce richer structures than WENO-Z, WENO-M and WENO-JS. It is noted that smaller vortices in the WENO-MS result have combined into larger vortices such that the resolution looks lower but actually is higher than the P-WENO result and WENO-Z result. Again, the sequence of resolution is WENO-MS $\geq$ P-WENO $>$ WENO-Z $\geq$ WENO-M $>$ WENO-JS. The present results are comparable to those in Ref. [8].

2. 2D Rayleigh–Taylor Instability Taylor instability happens on an interface between two fluids of different densities when an acceleration is directed from the heavier fluid to the lighter fluid. The problem has been widely used to test the numerical dissipation of a numerical scheme [8,21]. The computational domain is $[0, 0.25] \times [0, 1]$ and the initial conditions are

$$(\rho, u, v, p) = \begin{cases} (2, 0, -0.025a\cos(8\pi x), 2y + 1), & \text{if } 0 \le y < 0.5, \\ \left(1, 0, -0.025a\cos(8\pi x), y + \frac{3}{2}\right), & \text{if } 0.5 \le y \le 1.0, \end{cases} \tag{54}$$

where the sound speed $a = (\gamma p/\rho)^{1/2}$ and the ratio of specific heats $\gamma = 5/3$. The gravitational effect is introduced by adding the source term $S = (0, 0, \rho, \rho v)^T$ to the right-hand side of the 2D Euler equations (52). Reflective boundary conditions are imposed for the left and right boundaries, and the top and bottom boundaries are set as

$$(\rho, u, v, p) = \begin{cases} (2, 0, 0, 2.5), & \text{bottom-boundary}, \\ (1, 0, 0, 1), & \text{top-boundary}. \end{cases} \tag{55}$$

The density contours at the time $t = 1.95$ computed with different schemes are shown in Fig. 10. We see that the WENO-MS scheme generates more complex structures than the other schemes (e.g., more wiggles on the hat in Fig. 10e), indicating that it is less dissipative than the other schemes.

3. Double Mach Reflection of a Strong Shock [21] This problem is widely used to verify the performance of numerical methods. We calculate this test problem on the $[0, 4] \times [0, 1]$ domain and display the results in $[0, 3] \times [0, 1]$ as customary. Initially a right-moving Mach 10 shock wave is imposed and the shock front makes an angle of 60° with the x-axis at $x = 1/6$. The region from $x = 0$ to $x = 1/6$ along the bottom boundary is always assigned the exact post-shock states and the region $x \in [1/6, 4]$ is a reflecting wall. The left boundary is assigned the initial post-shock states. For the right boundary at $x = 4$, all gradients are set to zero. The top boundary of the problem is set to describe the exact motion of the Mach 10 shock. See [18] for a detailed description of this problem. We solve it up to time $t = 0.2$ using $\Delta x = \Delta y = 1/240$ with $\gamma = 1.4$. The numerical results of different schemes are compared in Fig. 11. Figure 12 shows the details at the Mach stem zone of the density variable. It can be clearly seen that WENO-MS scheme resolves better

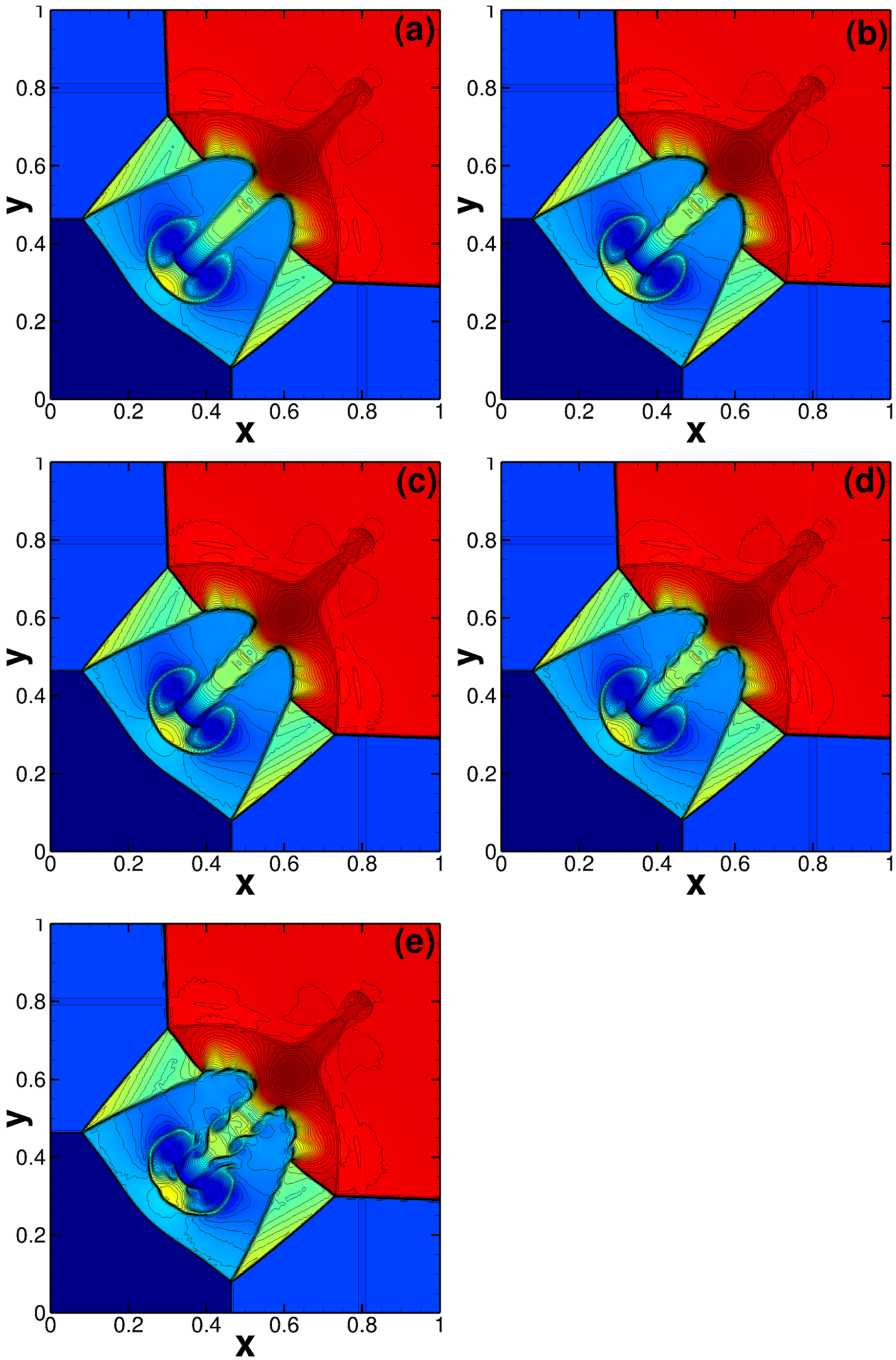

Fig. 8 Density contours of the 2D Riemann problem at $t = 0.8$ using 400×400 cells. **a** WENO-JS, **b** WENO-M, **c** WENO-Z, **d** P-WENO, **e** WENO-MS

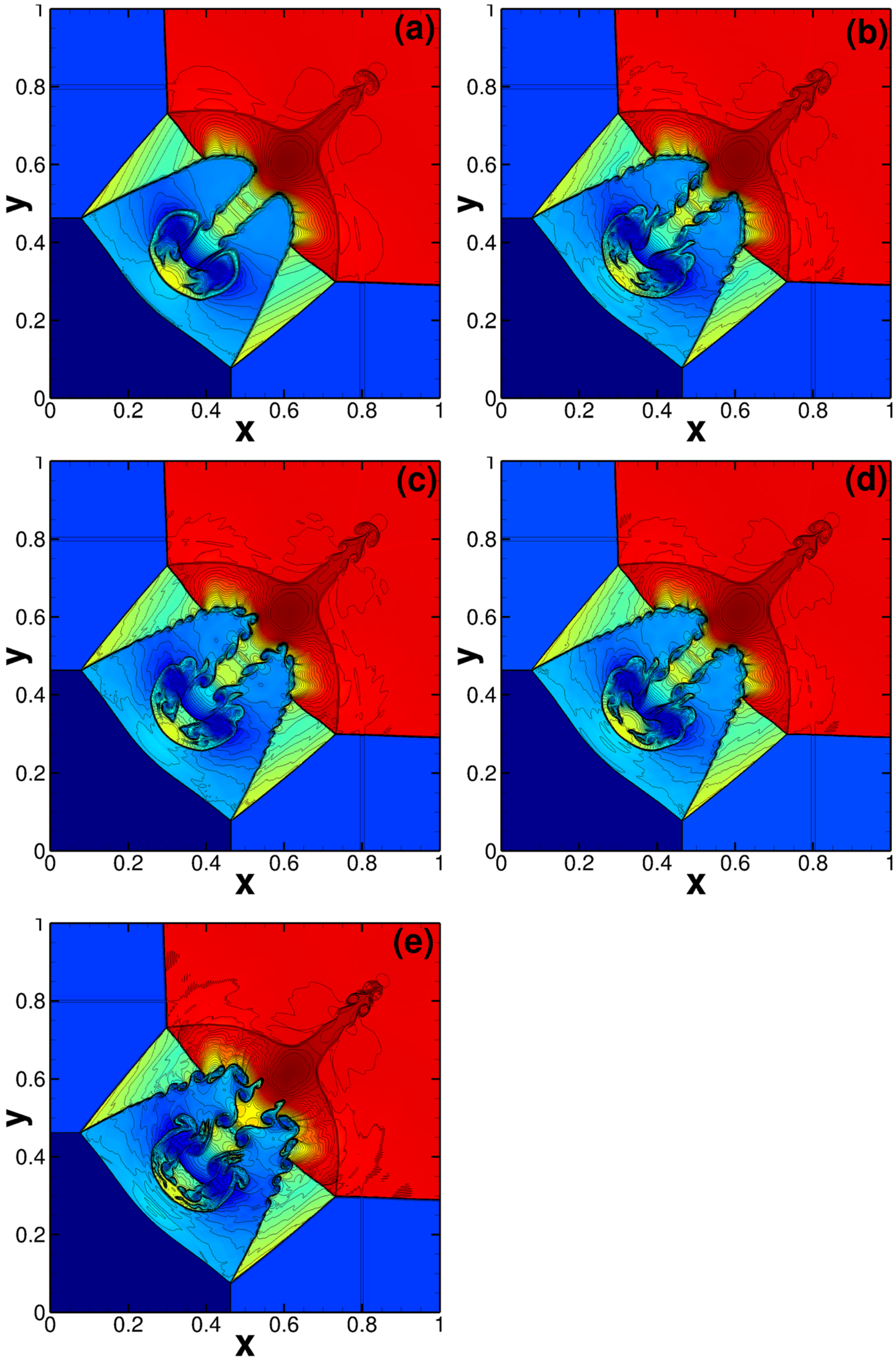

Fig. 9 Density contours of the 2D Riemann problem at $t = 0.8$ using 800×800 cells. **a** WENO-JS, **b** WENO-M, **c** WENO-Z, **d** P-WENO, **e** WENO-MS

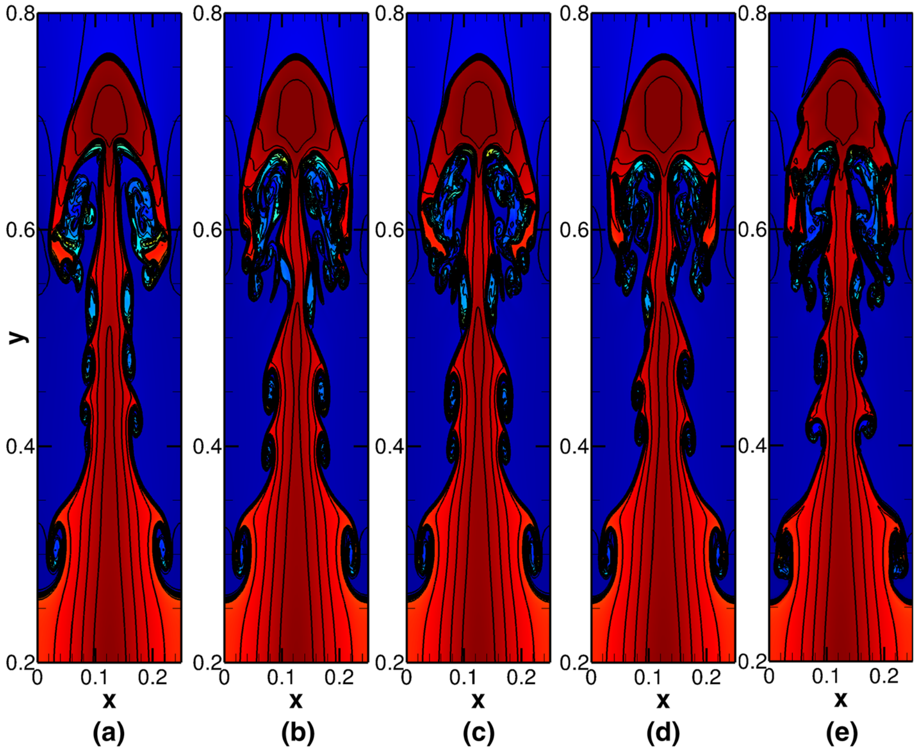

Fig. 10 Density contours of the Rayleigh–Taylor instability problem at $t = 1.95$ computed on 240×960 grids cells with **a** WENO-JS, **b** WENO-M, **c** WENO-Z, **d** P-WENO, **e** WENO-MS

the instabilities around the Mach stem than the other schemes, e.g., in Fig. 12d, vortices begin to form in more upstream position of the contact discontinuity than in (a),(b),(c) and (e).

5 Conclusions

We introduce a modified fifth-order WENO scheme (WENO-MS) by increasing the quadratic approximation polynomials of flux function on candidate stencils to cubic ones with information on the global 5-point stencil of the classical WENO scheme. The corresponding smoothness indicators are given and are used in the classic JS weights. To regain the ENO property, the effect of the additional high-order corrections are limited by a tunable function if any of the candidate stencils is discontinuous. Theoretical analysis and numerical results show that the new scheme can obtain the full fifth-order accuracy in smooth regions and at first-order critical points. Numerical experiments show that the proposed WENO-MS scheme resolves the fine smooth structures as well as or even better than the improved WENO schemes (P-WENO, WENO-Z, WENO-M) and the classic WENO-JS scheme, is robust for shock capturing, and increases only 7% of CPU time compared with the classical WENO-JS scheme.

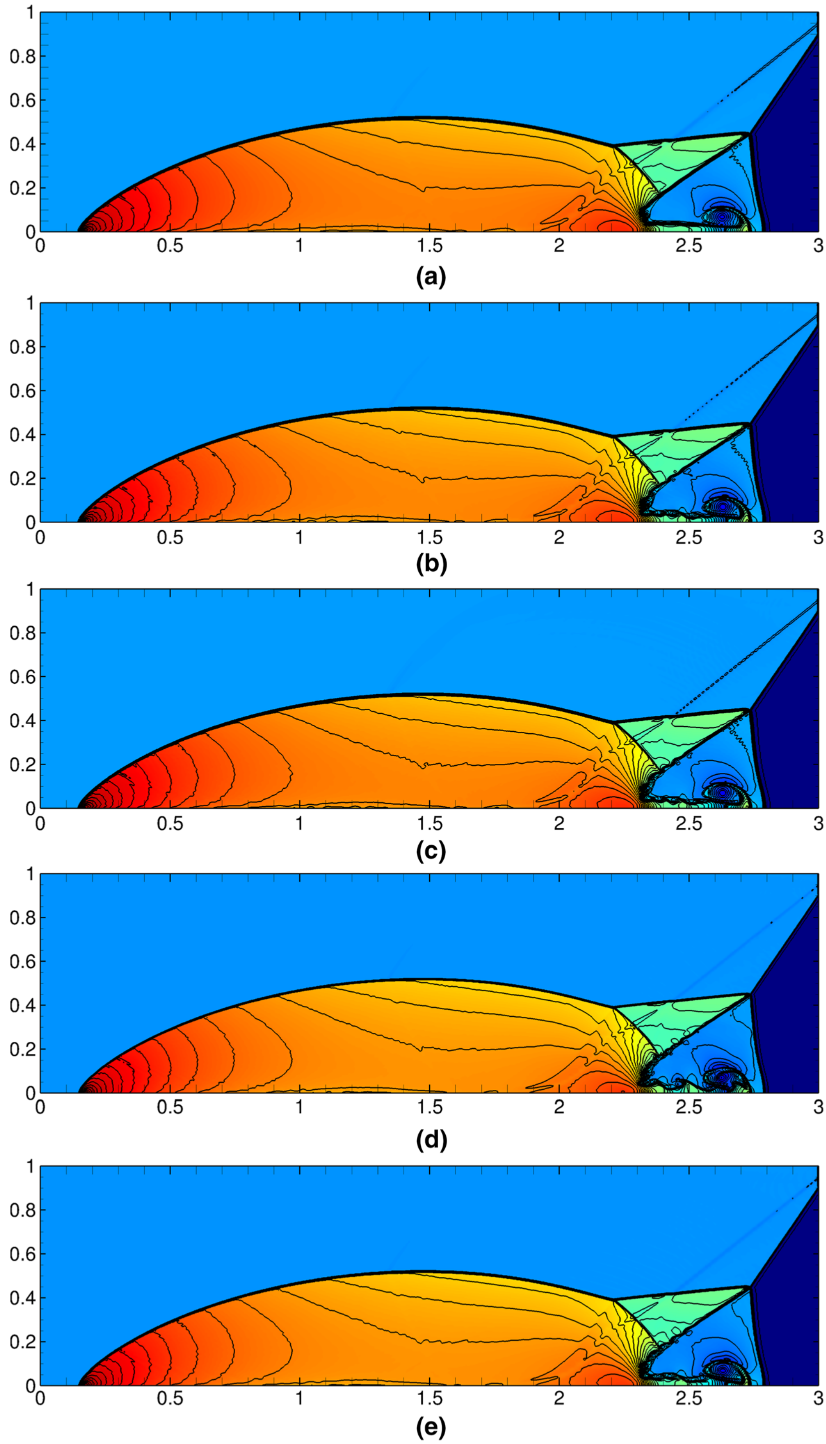

Fig. 11 Density contours of the double Mach reflection problem with 50 equally spaced contours at $t = 0.2$ computed on 960×240 grid cells with **a** WENO-JS, **b** WENO-M, **c** WENO-Z, **d** WENO-MS, **e** P-WENO

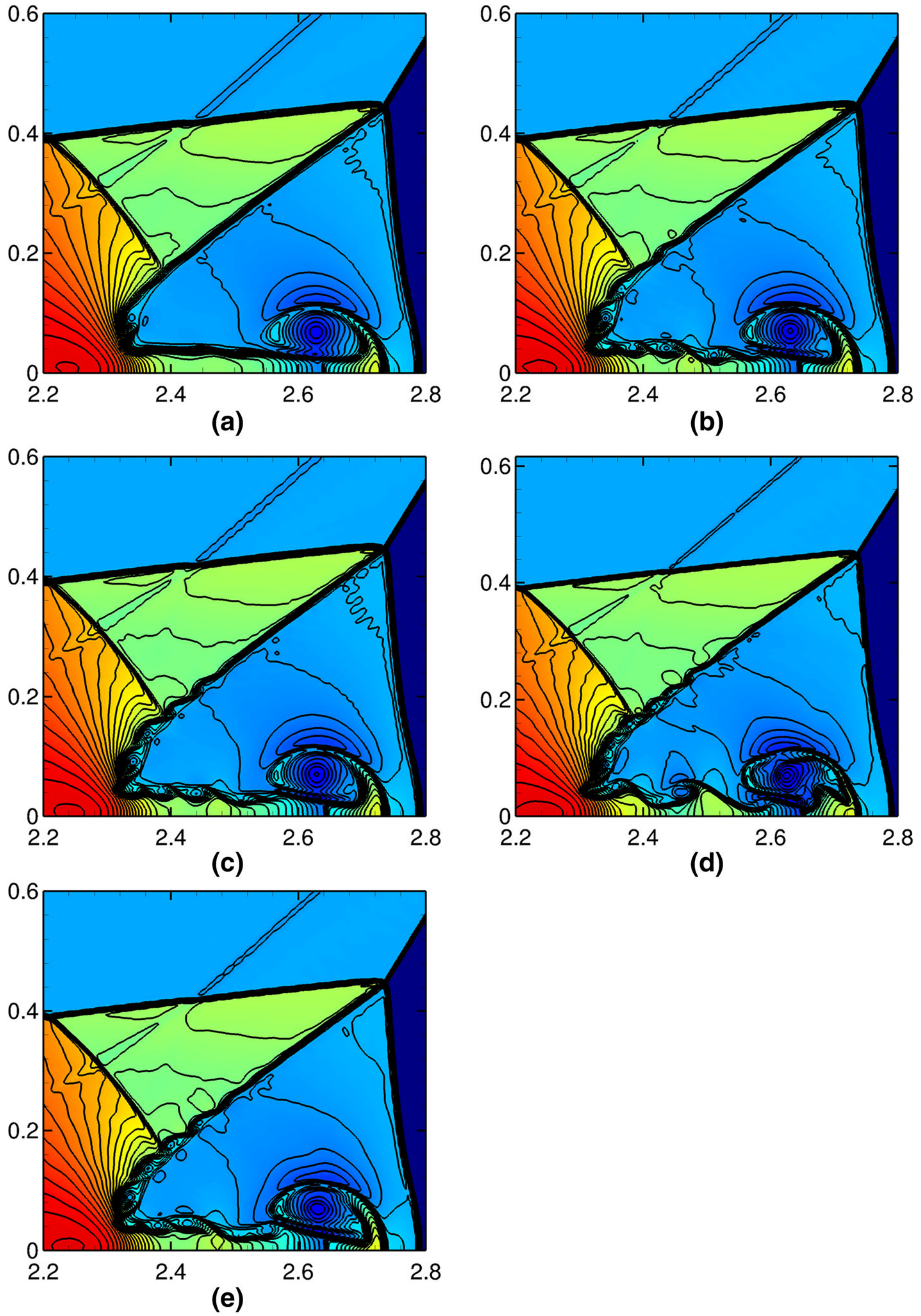

Fig. 12 Zoom in the region [2.2, 2.8] × [0, 0.6] near the Mach stem in Fig. 11 for double Mach reflection problem at $t = 0.2$ computed on 960 × 240 grids cells with **a** WENO-JS, **b** WENO-M, **c** WENO-Z, **d** WENO-MS, **e** P-WENO

Acknowledgements This work is supported by Natural Science Foundation of China (11261160486, 91641107, 91852116), Fundamental Research of Civil Aircraft (MJ-F-2012-04).

References

1. Harten, A.: High resolution schemes for hyperbolic conservation laws. J. Comput. Phys. **49**, 357–393 (1983)
2. Harten, A., Engquist, B., Osher, S., Chakravarthy, S.: Uniformly high-order accurate non-oscillatory schemes III. J. Comput. Phys. **71**, 231–303 (1987)
3. Liu, X.D., Osher, S., Chan, T.: Weighted essentially non-oscillatory schemes. J. Comput. Phys. **115**, 200–212 (1994)
4. Jiang, G.S., Shu, C.W.: Efficient implementation of weighted ENO schemes. J. Comput. Phys. **126**, 202–228 (1996)
5. Henrick, A.K., Aslam, T.D., Powers, J.M.: Mapped weighted-essentially-non-oscillatory schemes: achieving optimal order near critical points. J. Comput. Phys. **207**, 542–567 (2005)
6. Borges, R., Carmona, M., Costa, B., Don, W.S.: An improved WENO scheme for hyperbolic conservation laws. J. Comput. Phys. **227**, 3191–3211 (2008)
7. Ha, Y., Kim, C.H., Lee, Y.J., Yoon, J.: An improved weighted essentially non-oscillatory scheme with a new smoothness indicator. J. Comput. Phys. **232**, 68–86 (2013). https://doi.org/10.1016/j.jcp.2012.06.016
8. Kim, C.H., Ha, Y., Yoon, J.: Modified non-linear weights for fifth-order weighted essentially non-oscillatory schemes. J. Sci. Comput. **67**, 299–323 (2016). https://doi.org/10.1007/s10915-015-0079-3
9. Castro, M., Costa, B., Don, W.S.: High order weighted essentially non-oscillatory WENO-Z schemes for hyperbolic conservation laws. J. Comput. Phys **230**, 1766–92 (2011)
10. Arandiga, F., Baeza, A., Belda, A.M., Mulet, P.: Analysis of WENO schemes for full and global accuracy. SIAM J. Numer. Anal. **49**, 893–915 (2011)
11. Don, W.S., Borges, R.: Accuracy of the weighted essentially non-oscillatory conservative finite difference schemes. J. Comput. Phys. **250**, 347–72 (2013)
12. Zeng, F.J., Shen, Y.Q., Liu, S.P.: A perturbational weighted essentially non-oscillatory scheme. Comput. Fluids **172**, 196–208 (2018). https://doi.org/10.1016/j.compfluid.2018.07.003
13. Shu, C.W., Osher, S.: Efficient implementation of essentially non-oscillatory shock capturing schemes II. J. Comput. Phys. **83**, 32–78 (1989)
14. Shu, C.W.: Essentially non-oscillatory and weighted essentially non-oscillatory schemes for hyperbolic conservation laws. NASA/CR–97–206253, ICASE report no. 97–65
15. Shu, C.W., Osher, S.: Efficient implementation of essentially non-oscillatory shock capturing schemes. J. Comput. Phys. **77**, 439–471 (1988)
16. Lax, P.D.: Weak solutions of nonlinear hyperbolic equations and their numerical computation. Commun. Pure Appl. Math. **7**, 159–193 (1954)
17. Sod, G.: A survey of several finite difference methods for systems of nonlinear hyperbolic conservation laws. J. Comput. Phys. **27**, 1–31 (1978)
18. Woodward, P., Colella, P.: The numerical simulation of two-dimensional fluid flow with strong shocks. J. Comput. Phys. **54**, 115–173 (1984)
19. Pirozzoli, S.: Conservative hybrid compact-WENO schemes for shock-turbulence interaction. J. Comput. Phys. **178**, 81–117 (2002)
20. Schulz-Rinne, C.W., Collins, J.P., Glaz, H.M.: Numerical solution of the Riemann problem for two-dimensional gas dynamics. SIAM J. Sci. Comput. **14**(6), 1394–1414 (1993)
21. Glimm, J., Grove, J., Li, X.L., Oh, W., Tan, D.C.: The dynamics of bubble growth for Rayleigh–Taylor unstable interfaces. Phys. Fluids **31**, 447–465 (1988)